Pulmonary Functional Imaging

Structural and Functional Pulmonary Magnetic Resonance Imaging in Pediatrics—From the Neonate to the Young Adult

Laura L. Walkup, PhD, Nara S. Higano, PhD, Jason C. Woods, PhD

The clinical imaging modalities available to investigate pediatric pulmonary conditions such as bronchopulmonary dysplasia, cystic fibrosis, and asthma are limited primarily to chest x-ray radiograph and computed tomography. As the challenges that historically limited the application of magnetic resonance imaging (MRI) to the lung have been overcome, its clinical potential has greatly expanded. In this review article, recent advances in pulmonary MRI including ultrashort echo time and hyperpolarized-gas MRI techniques are discussed with an emphasis on pediatric research and translational applications.

Key Words: Pulmonary; MRI; Pediatrics.

© 2018 The Association of University Radiologists. Published by Elsevier Inc. All rights reserved.

INTRODUCTION

Pulmonary morbidity in infants and young children may arise from many sources: preterm birth (eg, bronchopulmonary dysplasia [BPD]), congenital defects such as congenital diaphragmatic hernia (CDH), genetic conditions such as cystic fibrosis (CF) which is now diagnosed at birth, and multitudinous airway obstruction such as asthma. Chest x-ray radiographs, often the first line of radiological inquiry to assess acute morbidity, are fast and easily deployable in the clinic; however, the modality lacks tomographic resolution. When higher precision is needed, chest x-ray computed tomography (CT) may be ordered; however, the modality is used sparingly in young patients, in part due to the need for sedation or anesthesia. Further, ionizing-radiation exposure remains a consideration for sensitive patients such as infants, immunocompromised patients, and children with chronic morbidities who may need many CT scans throughout their lifetime (1−3). With a mean lung dose of ~10 mGy per chest CT for patients under 5 years old, it has been projected that one radiation-induced solid cancer will result from every ~360 and every ~1200 chest CT scans for girls and boys, respectively (2). Though these risk assessments remain the subject of debate and need reevaluation in light of newer low-dose CT protocols, alternative modalities that are free of ionizing radiation would greatly expand the applications of imaging for longitudinal assessment of pediatric lung disease to study the natural history of pulmonary conditions that are poorly understood. Furthermore, there is additional opportunity for quantitative imaging to serve as a novel biomarker to evaluate individual patients' therapeutic response and for clinical trials of new therapeutics—especially in situations where patient numbers may be inherently small (eg, rare genotypes of CF and rare-lung diseases).

Magnetic resonance imaging (MRI), which is nonionizing and tomographic, is a strong candidate to fill this need; as the limitations that once hindered the clinical application of pulmonary MRI are overcome (ie, now submillisecond echo times [TE] that compensate for the fast $T_2^\star$ decay and acquisition strategies that are robust to cardiorespiratory motion), MRI is experiencing a renaissance as a viable modality for imaging the lungs. In this review, recent developments in the pediatric applications of pulmonary MRI are discussed, including results presented at the 2017 International Workshop on Pulmonary Imaging, with particular focus on ultrashort echo time (UTE) and hyperpolarized-gas MRI techniques for assessing structural and functional pathologies of pediatric lung diseases.

ULTRASHORT ECHO TIME MRI

Historically, MRI has not been used to image lung structure due to several challenges, including the inherently low proton density in lung parenchyma ($\sim$20% that of soft tissues in adults) (4) and the short $T_2^\star$ relaxation time in pulmonary tissues ($\sim$0.5−3 ms at typical field strengths) (4−8); these constraints historically have led to pulmonary MR images that contain little to no lung signal. Further, in general MRI is time-inefficient compared to other standard modalities, making it more susceptible to respiratory/cardiac motion and bulk-motion artifacts (9), which are especially prevalent in noncompliant subjects such as infants and young children.

These challenges are being overcome by technical development, and traditional proton MRI is emerging as a viable modality for structural lung imaging in infants and children, the former of which are arguably the most difficult patient population to image (10). Recently, changes in lung volume were assessed between fetal and postnatal imaging in infants with CDH, as were differences in lung growth between the ipsilateral and contralateral lungs after postnatal diaphragm repair (11). Faster growth in the contralateral lung versus ipsilateral was reported, and increased weight gain was associated with increased ipsilateral lung growth. Walkup et al recently demonstrated initial successes in quantitatively differentiating between neonates with and without BPD (12). Additionally, global morphology and perfusion scores from MRI were as sensitive as lung clearance index (LCI) in detecting response to antibiotic therapies in CF patients (13). However, conventional Cartesian sequences as used in the previous studies are still susceptible to the challenges of subject motion and short spin relaxation times, due to TE values that are often longer than the short $T_2^\star$, and thus cannot effectively visualize short-$T_2^\star$ tissues (ie, nonfibrotic parenchyma) in the lung. Therefore, the future of pulmonary MRI likely lies with sequences that are more robust to motion and implement a shorter TE value.

Recent, widespread development in radial/spiral UTE MR acquisition sequences for pulmonary imaging have allowed for progress beyond conventional Cartesian acquisitions (14−16). These sequences allow for near-immediate data acquisition after radio-frequency (RF) excitation of the nuclear spins, which provides an obvious advantage for short-$T_2^\star$ species such as lung tissue. The lung also has a relatively long T_1 ($\sim$1 second at 1.5 T) (17,18), so when UTE acquisitions are combined with small flip angles, UTE images with normalized lung intensities can provide a CT-like proton-density regime (19), which allows for improved quantification. While CT attenuation can be converted directly to volumetric density (from Hounsfield units to g/cm^3), signal intensity from the lung parenchyma in UTE images must first be normalized to the intensity of soft tissue to perform similar quantitative density analysis. Recent work on neonatal imaging has demonstrated that UTE MRI and CT provide similar lung parenchymal-tissue quantification and similar radiological reads in pathological regions containing, for example, cysts, ground glass opacities, fibrous/interstitial abnormalities, and consolidations (20). Such parenchymal-density quantification via MRI may be particularly important for chronically diseased children who may need serial imaging; quantification provides an objective means of assessing disease progression.

In addition to a parenchymal proton-density regime, UTE MRI provides additional advantages related to subject motion, which is a major consideration in light of both the longer exam times of MRI relative to CT and also the poor subject compliance in pediatric populations. Due to oversampling near the center of k-space, radial sequences are more robust to motion than Cartesian sequences (21). In addition, radial UTE MRI has inherent self-navigation via the k-space center that allows for retrospective tracking of bulk motion; data acquired during noncompliant intervals can be discarded, and images with diagnostic quality can be reconstructed from the remaining quiescent data (19). Further, this self-navigation allows for retrospective respiratory gating (22−24). Data acquired from a free-breathing neonate can be binned and reconstructed into representative end-expiration and end-inspiration frames without breath-holds (Fig 1) (25), which may be important in assessing tidal volumes, regional lung compliance, ventilation mapping, and hyperinflation in certain conditions such as BPD, or diaphragmatic function before and after operative repairs in patients with CDH. The ability to perform respiratory gating in a free-breathing infant is highly beneficial, as rapid respiratory tracking in neonates has been challenging historically (19). This inherent motion-tracking technique is very important for a noncompliant neonatal and infant populations because it obviates the necessity of sedation/anesthesia—a clear advantage over CT given the rising concerns over the effects of anesthesia in children (26).
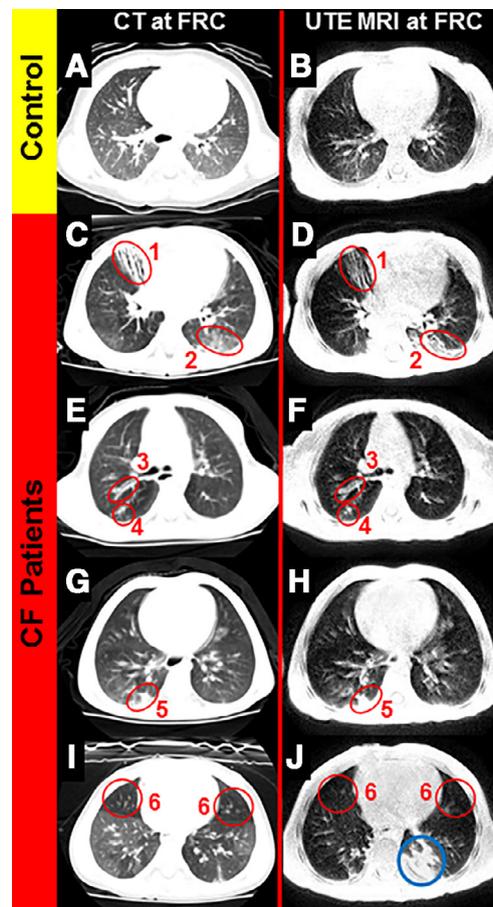
UTE MRI also performs comparably with CT in pediatric CF patients to evaluate early disease. Recent studies have demonstrated better agreement between MRI and CT with radial UTE sequences (such PETRA, or pointwise encoding time reduction with radial acquisition) than with conventional T_1- or $T_2^\star$-weighted sequences (16), and additionally, agreement between different MRI scoring systems for CF (27). Dournes et al demonstrated submillimeter 3D MRI of the airways of pediatric and young adult CF patients using PETRA and found good agreement between CT and PETRA using the Helbich-Bhalla scoring as compared to conventional sequences (28). Roach et al recently demonstrated comparable disease detection in $\sim$1−4-year-old CF patients (Fig 2) and a significant correlation between CT- and UTE MRI-derived scores in this young population ($p < 0.001$) using previously validated CF scoring systems for CT and UTE MRI (29). The results of these studies support the integration of UTE MRI into routine clinical exams for more comprehensive evaluation of early CF lung disease.

Pulmonary MRI has the potential to deepen our understanding of neonatal and pediatric lung diseases and their
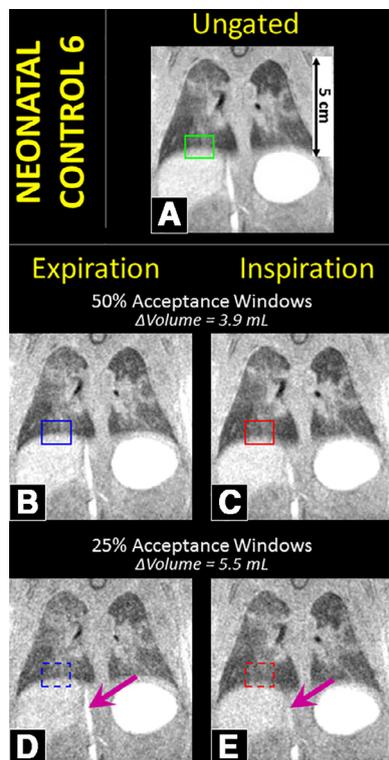
Fig. 1. Coronal views of 3D UTE MR images in a neonatal control patient demonstrating ungated reconstructions (A) and retrospectively respiratory-gated reconstructions at 50% and 25% acceptance windows for end-expiration (B and D) and end-inspiration (C and E). The boxes indicate a region of lung-diaphragm transition, and the *arrows* indicate the inferior vena cava, the movement of which is more finely resolved in the 25%-windowed images. A tidal volume measurement—not easily assessed in infants by any clinical means—is measured via the segmentation of these images. Reprinted from Ref (19) "Retrospective respiratory self−gating and removal of bulk motion in pulmonary UTE MRI of neonates and adults," Nara S. Higano, Andrew D. Hahn, Jean A. Tkach, Xuefeng Cao, Laura L. Walkup, Robert P. Thomen, Stephanie L. Merhar, Paul S. Kingma, Sean B. Fain, and Jason C. Woods, Magnetic Resonance in Medicine, 2017, Volume 77, pages 1284−1295, with permission from John Wiley and Sons. MR, magnetic resonance;UTE, ultrashort echo time.

Fig. 2. Slice-matched comparison of axial x-ray CT (left column) and UTE MR (right column) images of infants with cystic fibrosis and a control (ages 33−47 months old), demonstrating how both CT and UTE MRI can visualize CF pathology: bronchiectasis (1), ground-glass opacity (2), bronchial-wall thickening (3), mucus plugging (4), consolidation (5), and air trapping (6). Anesthesia-induced atelectasis is circled in the blue. Reprinted from Ref (29) with permission of the American Thoracic Society. Copyright 2017 American Thoracic Society. David J. Roach, Yannick Crémillieux, Robert J. Fleck, Alan S. Brody, Suraj D. Serai, Rhonda D. Szczesniak, Stephanie Kerlakian, John P. Clancy, and Jason C. Woods, 2016, "Ultrashort Echo-Time Magnetic Resonance Imaging Is a Sensitive Method for the Evaluation of Early Cystic Fibrosis Lung Disease", Annals of the American Thoracic Society Volume 13, Issue 11, pages 1923−1931. Annals of the American Thoracic Society is an official journal of the American Thoracic Society. CF, cystic fibrosis; CT, computed tomography; MR, magnetic resonance; UTE, ultrashort echo time. Color version of figure is available online.

time−courses. BPD is a common and serious pulmonary complication of premature birth, but the underlying pathology of the disease, its trajectory over time, and clinical outcomes relative to initial condition are not well characterized. Recent work with radiological scoring of UTE and short−TE gradient echo MRI of neonatal patients with BPD has demonstrated that structural MRI in early life has predictive capability in identifying preterm infants at higher risk for respiratory morbidities; these preliminary results therefore support the wider implementation of early−life MRI as a predictor of disease trajectories (30,31). Pulmonary UTE MRI has the potential to play a vital role in determining prognosis, evaluating efficacy of individualized therapies, and informing clinical management of neonatal and pediatric patients, and importantly can be implemented serially without requiring ionizing radiation, sedation, or anesthesia.

OTHER ¹H MRI TECHNIQUES

While this review focuses more on UTE and hyperpolarized−gas techniques, important progress also has been made using oxygen-enhanced proton MRI and Fourier-decomposition techniques; to date more progress has been reported in adults than pediatric populations, but both of these techniques have strong translational potential in pediatrics and could provide important functional information (ie, regional ventilation and perfusion) in conditions like BPD and CDH. Oxygen−enhanced techniques exploit the relationship between the

lung's T_1 relaxation and alveolar partial pressure of O_2; under hyperoxic conditions, the T_1 of the lungs is shorter relative to normoxia due to the increased concentration of paramagnetic O_2 in the alveolar airspaces. Difference maps are generated from two T_1-weighted image sets acquired under normoxic- (21% O_2) and hyperoxic- (100% O_2) breathing conditions, and differences in signal intensity (a maximum of about 6%) are attributed to ventilation (32,33). Kruger et al demonstrated using a 3D-radial UTE pulse sequence to acquire oxygen-enhanced images in healthy adult subjects (34), and recently, this approach was used to perform oxygen-enhanced MRI in adults with asthma and CF and demonstrated smaller signal-intensity enhancements in these disease groups relative to controls (35).

Fourier-decomposition MRI began with the realization that in a continuous proton acquisition over many heartbeats and breaths, images could be reconstructed with Fourier components at the breathing frequency and heart rate separately, providing qualitative images of ventilation and perfusion, respectively, without contrast agents or respiratory gating (36). Initial criticisms focused on the lack of quantitation and the fact that nonlung tissue provided ventilation signal because there was respiratory-related movement in the liver, for example. Recent work has focused on quantitative analysis; Kjùrstand et al reported using the zero-frequency image from the Fourier analysis as a baseline for ventilation quantification in healthy adult subjects and those with lung cancer (37). While most clinical Fourier-decomposition MRI studies to date have been performed in adults and are beyond the scope of this review (the interested reader is directed to Kjùrstand et al (38)), the technique has been reported in pediatric CF patients and was found to provide equivalent perfusion information to dynamic contrast-enhanced MRI but without the use of gadolinium (39).
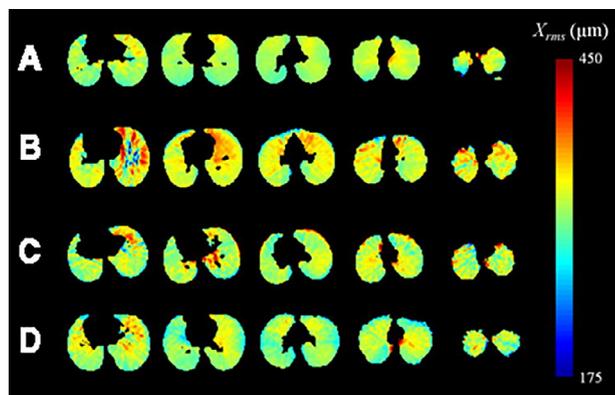
HYPERPOLARIZED-GAS MRI

Use of hyperpolarized noble gases (eg, [3]He or [129]Xe) as an inhaled contrast agent for MRI of the lung is not a novel technique; over the past 30 years, hyperpolarized-gas MRI, primarily with [3]He due to higher polarizability, has enjoyed wide research success in a range of adult lung diseases including asthma and chronic obstructive pulmonary disease (COPD) (40−43). The clinical accessibility of these techniques, however, has been stunted by several historical factors including the increasing scarcity of [3]He and intellectual-property claims (44,45). As a result, most of the hyperpolarized-gas MRI research has emerged from only a handful of institutions. In the last 10 years, rapid development and commercialization of polarizer technology (46−48) has allowed the less scarce [129]Xe to rise as a viable alternative to [3]He, and perhaps for the first time in its history, hyperpolarized-gas MRI sits on the precipice of widespread clinical translation.

While in-depth reviews of hyperpolarized-gas physics and translational applications can be found elsewhere (25,49−51), there are three broad categories of hyperpolarized-gas MRI

techniques: (i) static ventilation imaging, which visualizes regions in the lung airspaces filled by the inhaled gas during a breath hold; (ii) restricted-diffusion imaging, which uses diffusion-sensitizing gradients to measure how free Brownian motion of gas atoms is restricted by parenchymal tissue walls; and (iii) dissolved-phase imaging, which capitalizes on the solubility of [129]Xe in tissues and blood to measure gas transfer across the blood-gas barrier and uptake by red blood cells. Each of these methods plays into the ability of hyperpolarized gases to assess both the obstructive and restrictive components of lung disease, and recently several groups have expanded their hyperpolarized-gas MRI research efforts to include infants and young children.

In ventilation images, regions of the lung that are obstructed will appear darker than the signal mean; these so-called "ventilation defects" have been observed and quantified in numerous adult lung diseases including asthma and COPD. Koumellis et al used dynamic hyperpolarized [3]He ventilation MRI to quantify regional airway obstruction in a cohort of CF patients aged 6−15 years old and reported good correlation with forced expiratory volume in 1 second (FEV$_1$), a global lung function measurement from spirometry, which in this cohort corresponded to primarily upper-lobe obstruction (52). This regional information is the greatest advantage of hyperpolarized-gas MRI techniques over traditional pulmonary function tests. Recently, Thomen et al reported regional ventilation deficits in young CF patients (ages 8−16 years old); importantly, [129]Xe ventilation defects were observed even in CF patients with mild disease and normal FEV$_1$, and quantification of these defects differentiated CF patients from age-matched controls where FEV$_1$ could not, supporting the increased sensitivity of hyperpolarized [129]Xe MRI compared to spirometry (53). Recently, Kanhere et al demonstrated a strong correlation between LCI as measured with multiple-breath N$_2$ washout and hyperpolarized [129]Xe ventilation defect percentage, suggesting that both techniques assess similar pathophysiologic characteristics of CF and opening the door for future multiple-breath wash-in and wash-out [129]Xe MR imaging to investigate the temporal dynamics of ventilation (54).

Airway obstruction may also arise from elastic-recoil mismatch between inspiration and expiration, as seen as air trapping and emphysema typical of COPD; while emphysema is not a common pediatric diagnosis, emphysema-like airspace enlargement has been noted in CT scans of children and young adults with CF and BPD (55−57), and this enlargement can be quantified via an apparent diffusion coefficient (ADC) measured with restricted-diffusion hyperpolarized-gas imaging. A recent study performed hyperpolarized [3]He restricted diffusion MRI in a small cohort of young adult CDH patients and reported significantly elevated ADC consistent with enlarged alveolar airspaces in the ipsilateral lung relative to the contralateral lung. [3]He ventilation MRI also found ventilation defects in the ipsilateral lung, in addition to smaller ventilated lung volume than the contralateral lung, suggesting some obstructive component to CDH (58). While

Fig. 3. Maps of the root-mean-square diffusion length (χ_{rms}, a measurement of alveolar-airspace size) of hyperpolarized ^{3}He in four pediatric subjects (9-10 years old). In this study, children with a history of wheezing illness with human rhinovirus (HRV) infection in early childhood (Subjects C and D) had smaller airways as compared to those who did not (Subjects A and B). Reprinted from Ref (59), 2013 with permission from Elsevier.

these subjects were older (median age 29 years old), the results speak to the ability of hyperpolarized-gas MRI techniques to assess both the microstructural and functional abnormalities in congenital disorders of the lung such as CDH. In childhood asthma, Cadman et al reported a greater degree of hyperpolarized-^{3}He restricted gas diffusion and ventilation deficits in children aged 9−10 years with asthma compared to those without asthma, suggestive of relatively smaller alveolar airspaces in the former; furthermore, asthmatic children with a history of wheezing illness with rhinovirus infection before age 3 had higher ^{3}He ventilation defect scores and lower diffusion length compared to asthmatic children who did not (Fig 3), linking wheezing in early childhood, a known risk factor, to a microstructural biomarker of the alveolar airspaces (59). Recently, Fishman et al demonstrated that alveolar depth as measured with ^{3}He diffusion MRI

correlated with lung lifespan in a small group of pediatric lung-transplant recipients, ie, patients whose lungs had a more shallow alveolar depth had a negative outcome (death or retransplantation) sooner than those with greater alveolar depth, supporting hyperpolarized-gas MRI as a means of predicting outcomes for lung-transplant patients and as an aid for lung selection for transplantation (60).

One of the largest challenges of extending hyperpolarized-gas MRI methods down to the neonate and infant is the inhalation and breath-hold of the hyperpolarized gas, which in a compliant pediatric subject simply would be practiced and coached. Using a pediatric-sized bag valve mask and a rapid 2D-interleaved spiral pulse sequence, Altes et al at University of Virginia presented a proof-of-concept study demonstrating the feasibility of hyperpolarized ^{3}He MRI in nonsedated children as young as 2 months old. ^{3}He ventilation defects were observed in a 2-month-old prematurely born infant, two CF patients (10 and 14 months old), and two 3-year olds with asthma (Fig 4) (61). In addition to functional abnormalities, Higano et al reported alveolar microstructural changes observed via hyperpolarized ^{3}He diffusion MRI of explanted neonatal and infant lungs. While most of the samples were from healthy infants without known pulmonary disease, in one case of filamin A deficiency (a rare genetic mutation associated with diffuse lung disease (62)), ^{3}He ADC measurements were noticeably larger than those of the control samples, indicative of abnormally enlarged alveolar airspaces; these ADC measurements correlated significantly with measurements from quantitative histology (63).

These hyperpolarized-gas MRI studies demonstrate that the microstructural and functional abnormalities of pediatric conditions such as BPD, CDH, asthma, and CF begin in very early life and that there is great potential for hyperpolarized-gas MRI to monitor disease progression during early ages when spirometry and other pulmonary function tests are not feasible or reproducible, to individualize care management,
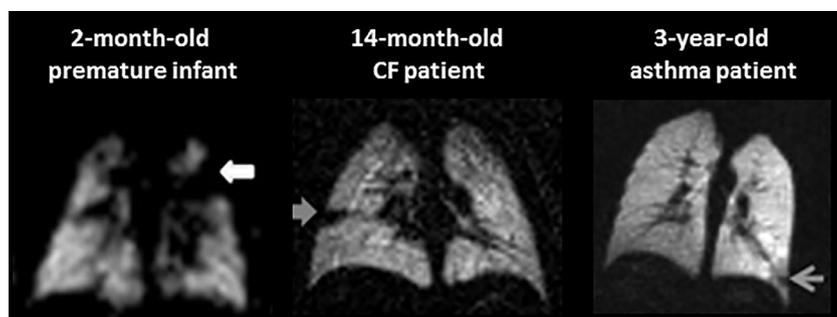
Fig. 4. Hyperpolarized ^{3}He ventilation MR images in three nonsedated, nonrestrained young children demonstrating early ventilation deficits (arrows) associated with premature birth, CF, and asthma. Figure is a composite of images reprinted from Ref (61), Clinical Imaging, 2017, Volume 45, pages 105−110, "Hyperpolarized helium-3 magnetic resonance lung imaging of nonsedated infants and young children: a proof-of-concept study", Talissa A. Altes, Craig H. Meyer, Jaime F. Mata, Deborah K. Froh, Alix Paget-Brown, W. Gerald Teague, Sean B. Fain, Eduard E. de Lange, Kai Ruppert, Martyn C. Botfield, Mac A. Johnson, John P. Mugler (https://doi.org/10.1016/j.clinimag.2017.04.004) with permission from Elsevier under the Creative Commons license (HYPERLINK" https://creativecommons.org/licenses/by-nc-nd/4.0/). CF, cystic fibrosis; MR, magnetic resonance.

and perhaps even to predict outcomes for these children who are likely to face lifelong pulmonary complications. While hyperpolarized-gas MRI alone cannot discern the structural etiology of a functional deficit (ie, if a regional ventilation defect arises from mucus plugging or bronchiectasis), these techniques may be used in conjunction with structural imaging such as CT or UTE MRI to identify regional lung macrostructural-functional correlates.

DISCUSSION

As lung MRI techniques with previous successes in adult medicine are moved to younger populations, it is clear that there is ample opportunity for MRI to revolutionize the imaging and clinical management of pediatric pulmonary conditions. While momentum and enthusiasm for pulmonary MRI of infants and young children is growing, some challenges remain for broader clinical translation. For instance, while UTE MRI is capable of very high 3D-spatial resolution, it will likely never meet or surpass the resolution achievable with x-ray CT, and while CT will likely continue to be the preferred modality for clinical assessments in the short term, MRI will have an advantage for longitudinal studies of pediatric lung conditions as accumulated ionizing-radiation exposure is a nonissue with MRI.

For the imaging of particularly vulnerable patients, such as neonates or those in intensive care units, scanner location can be particularly important for logistics and safety. Thus, several major pediatric hospitals are looking to add MRI capabilities soon in or near their neonatal intensive care wards. Further, all three major MRI-scanner manufacturers (ie, Philips, GE, and Siemens) either have a UTE pulse sequence available or plan to make one available soon, which will improve the clinical translation of UTE methods for the pulmonary imaging of all patient populations. Quantification of UTE images will likely remain a tool for research studies until image processing and segmentation techniques are fully automated; however, as clinician familiarity with UTE techniques increases, reader interpretation will likely be sufficient in the short term for clinical use.

Image processing is also a challenge for translating oxygen-enhanced MRI techniques to pediatric populations since the method requires two spatially registered image sets which may be challenging to acquire in noncompliant patients, but perhaps retrospective-respiratory gating strategies as reviewed here may help overcome those challenges. One advantage of oxygen-enhanced MRI to evaluate ventilation is that the "contrast agent" is O_2, and thus, unlike the hyperpolarized gases, does not require a Food and Drug Administration (FDA) Investigational New Drug (IND) application.

The major remaining hurdles to widespread translation of hyperpolarized-gas MRI include polarizer access and FDA approval—indeed, these have been the technique's greatest challenges for the past three decades. However, accessibility to ^{129}Xe polarizers is improving, and recently the ^{129}Xe MRI Clinical Trials Consortium has emerged as a resource for groups interested in multisite clinical trials of hyperpolarized ^{129}Xe MRI (64). ^{129}Xe is already approved by the United Kingdom's Medicines and Healthcare products Regulatory Agency, and as more studies are conducted to assess the sensitivity of inhaled ^{129}Xe gas, US FDA approval becomes more likely, which will improve the accessibility and translation of these techniques to the clinic.

In conclusion, pulmonary UTE and hyperpolarized-gas MRI are poised to have large translational impact in the clinical diagnosis and care management of pediatric lung diseases by illuminating and quantifying regional structure-function relationships within the lungs, with clear relationships to outcomes.

REFERENCES

1. Brenner D, Elliston C, Hall E, et al. Estimated risks of radiation-induced fatal cancer from pediatric CT. AJR Am J Roentgenol 2001; 176:289–296.
2. Miglioretti DL, Johnson E, Williams A, et al. The use of computed tomography in pediatrics and the associated radiation exposure and estimated cancer risk. JAMA Pediatr 2013; 167:700–707.
3. Pearce MS, Salotti JA, Little MP, et al. Radiation exposure from CT scans in childhood and subsequent risk of leukaemia and brain tumours: a retrospective cohort study. Lancet 2012; 380:499–505.
4. Hatabu H, Alsop DC, Listerud J, et al. T2* and proton density measurement of normal human lung parenchyma using submillisecond echo time gradient echo magnetic resonance imaging. Eur J Radiol 1999; 29:245–252.
5. Ohno Y, Koyama H, Yoshikawa T, et al. T2* measurements of 3-T MRI with ultrashort TEs: capabilities of pulmonary function assessment and clinical stage classification in smokers. AJR Am J Roentgenol 2011; 197:W279–W285.
6. Stock KW, Chen Q, Hatabu H, et al. Magnetic resonance T2* measurements of the normal human lung in vivo with ultra-short echo times. Magn Reson Imaging 1999; 17:997–1000.
7. Theilmann RJ, Arai TJ, Samiee A, et al. Quantitative MRI measurement of lung density must account for the change in T(2) (*) with lung inflation. J Magn Reson Imaging 2009; 30:527–534.
8. Yu J, Xue Y, Song HK. Comparison of lung T2* during free-breathing at 1.5 T and 3.0 T with ultrashort echo time imaging. Magn Reson Med 2011; 66:248–254.
9. Stadler A, Schima W, Ba-Ssalamah A, et al. Artifacts in body MR imaging: their appearance and how to eliminate them. Eur Radiol 2007; 17:1242–1255.
10. Merhar SL, Tkach JA, Woods JC, et al. Neonatal imaging using an on-site small footprint MR scanner. Pediatr Radiol 2017; 47:1001–1011.
11. Schopper MA, Walkup LL, Tkach JA, et al. Evaluation of neonatal lung volume growth by pulmonary magnetic resonance imaging in patients with congenital diaphragmatic hernia. J Pediatr 2017; 188:96–102.e1.
12. Walkup LL, Tkach JA, Higano NS, et al. Quantitative magnetic resonance imaging of bronchopulmonary dysplasia in the neonatal intensive care unit environment. Am J Respir Crit Care Med 2015; 192:1215–1222.
13. Stahl M, Wielputz MO, Graeber SY, et al. Comparison of lung clearance index and magnetic resonance imaging for assessment of lung disease in children with cystic fibrosis. Am J Respir Crit Care Med 2017; 195:349–359.
14. Johnson KM, Fain SB, Schiebler ML, et al. Optimized 3D ultrashort echo time pulmonary MRI. Magn Reson Med 2013; 70:1241–1250.
15. Lederlin M, Cremillieux Y. Three-dimensional assessment of lung tissue density using a clinical ultrashort echo time at 3 tesla: a feasibility study in healthy subjects. J Magn Reson Imaging 2014; 40:839–847.
16. Dournes G, Grodzki D, Macey J, et al. Quiet submillimeter MR imaging of the lung is feasible with a PETRA sequence at 1.5 T. Radiology 2015; 276:258–265.
17. Kruger SJ, Fain SB, Johnson KM, et al. Oxygen-enhanced 3D radial ultrashort echo time magnetic resonance imaging in the healthy human lung. NMR Biomed 2014; 27:1535–1541.

18. Stadler A, Jakob PM, Griswold M, et al. T1 mapping of the entire lung parenchyma: Influence of the respiratory phase in healthy individuals. J Magn Reson Imaging 2005; 21:759–764.

19. Higano NS, Hahn AD, Tkach JA, et al. Retrospective respiratory self-gating and removal of bulk motion in pulmonary UTE MRI of neonates and adults. Magn Reson Med 2017; 77:1284–1295.

20. Higano NS, Fleck RJ, Spielberg DR, et al. Quantification of neonatal lung parenchymal density via ultrashort echo time MRI with comparison to CT. J Magn Reson Imaging 2017; 46:992–1000.

21. Hahn AD, Higano NS, Walkup LL, et al. Pulmonary MRI of neonates in the intensive care unit using 3D ultrashort echo time and a small footprint MRI system. J Magn Reson Imaging 2017; 45:463–471.

22. Triphan SMF, Breuer FA, Gensler D, et al. Oxygen enhanced lung MRI by simultaneous measurement of T1 and T2* during free breathing using ultrashort TE. J Magn Reson Imaging 2015; 41:1708–1714.

23. Weick S, Breuer FA, Ehses P, et al. DC-gated high resolution three-dimensional lung imaging during free-breathing. J Magn Reson Imag 2013; 37:727–732.

24. Tibiletti M, Paul J, Bianchi A, et al. Multistage three-dimensional UTE lung imaging by image-based self-gating. Magn Reson Med 2016; 75:1324–1332.

25. Walkup LL, Woods JC. Newer imaging techniques for bronchopulmonary dysplasia. Clin Perinatol 2015; 42:871–887.

26. Cravero JP, Beach ML, Blike GT, et al. The incidence and nature of adverse events during pediatric sedation/anesthesia with propofol for procedures outside the operating room: a report from the Pediatric Sedation Research Consortium. Anesthesia Analg 2009; 108:795–804.

27. Sileo C, Corvol H, Boelle PY, et al. HRCT and MRI of the lung in children with cystic fibrosis: comparison of different scoring systems. J Cystic Fibrosis 2014; 13:198–204.

28. Dournes G, Menut F, Macey J, et al. Lung morphology assessment of cystic fibrosis using MRI with ultra-short echo time at submillimeter spatial resolution. Eur Radiol 2016; 26:3811–3820.

29. Roach DJ, Cremillieux Y, Fleck RJ, et al. Ultrashort echo-time magnetic resonance imaging is a sensitive method for the evaluation of early cystic fibrosis lung disease. Ann Am Thorac Soc 2016; 13:1923–1931.

30. Higano NS, Fleck R, Spielberg DR, et al. Neonatal Pulmonary MRI of Bronchopulmonary Dysplasia Predicts Short-term Clinical Outcomes. Am J Respir Crit Care Med 2018; doi:10.1164/rccm.201711-2287OC. [epub ahead of print].

31. Higano NS, Spielberg DR, Fleck RJ, et al. Quantitative characterization of bronchopulmonary dysplasia severity using neonatal pulmonary MRI and correlation to short-term outcomes. Annual meeting of the Radiological Society of North America. Chicago, IL 2017.

32. Jakob PM, Wang T, Schultz G, et al. Assessment of human pulmonary function using oxygen-enhanced T1 imaging in patients with cystic fibrosis. Magn Reson Med 2004; 51:1009–1016.

33. Edelman RR, Hatabu H, Tadamura E, et al. Noninvasive assessment of regional ventilation in the human lung using oxygen-enhanced magnetic resonance imaging. Nat Med 1996; 2:1236.

34. Kruger SJ, Fain SB, Johnson KM, et al. Oxygen-enhanced 3D radial ultrashort echo time magnetic resonance imaging in the healthy human lung. NMR Biomed 2014; 27:1535–1541.

35. Zha W, Kruger SJ, Johnson KM, et al. Pulmonary ventilation imaging in asthma and cystic fibrosis using oxygen-enhanced 3D radial ultrashort echo time MRI. J Magn Reson Imaging 2017; 47:1287–1297.

36. Bauman G, Puderbach M, Deimling M, et al. Non-contrast-enhanced perfusion and ventilation assessment of the human lung by means of fourier decomposition in proton MRI. Magn Reson Med 2009; 62:656–664.

37. Kjùrstad À, Corteville DMR, Henzler T, et al. Quantitative lung ventilation using Fourier decomposition MRI; comparison and initial stud. Magn Reson Mater Phys, Biol Med 2014; 27:467–476.

38. Kjùrstad A, Regier M, Fiehler J, et al. A decade of lung expansion: a review of ventilation-weighted (1)H lung MRI. Z Med Phys 2017; 27:172–179.

39. Bauman G, Puderbach M, Heimann T, et al. Validation of Fourier decomposition MRI with dynamic contrast-enhanced MRI using visual and automated scoring of pulmonary perfusion in young cystic fibrosis patients. Eur J Radiol 2013; 82:2371–2377.

40. Altes TA, Powers PL, Knight-Scott J, et al. Hyperpolarized He-3 MR lung ventilation imaging in asthmatics: preliminary findings. J Magn Reson Imaging 2001; 13:378–384.

41. Kirby M, Svenningsen S, Kanhere N, et al. Pulmonary ventilation visualized using hyperpolarized helium-3 and xenon-129 magnetic resonance imaging: differences in COPD and relationship to emphysema. J Appl Physiol (1985) 2013; 114:707–715.

42. Qing K, Mugler 3rd JP, Altes TA, et al. Assessment of lung function in asthma and COPD using hyperpolarized 129Xe chemical shift saturation recovery spectroscopy and dissolved-phase MRI. NMR Biomed 2014; 27:1490–1501.

43. Capaldi DP, Sheikh K, Guo F, et al. Free-breathing pulmonary H and hyperpolarized He MRI: comparison in COPD and bronchiectasis. Acad Radiol 2014; 22:320–329.

44. Caught by surprise: causes and consequences of the Helium-3 supply crisis. Hearing before the US house of representatives, committee on science and technology. Washington, D.C.: US Government Printing Office, 2010.

45. Cho A. Helium-3 shortage could put freeze on low-temperature research. Science 2009; 326:778–779.

46. Driehuys B, Cates G, Miron E, et al. High-volume production of laser-polarized 129Xe. Appl Phys Lett 1996; 69:1668–1670.

47. Freeman MS, Emami K, Driehuys B. Characterizing and modeling the efficiency limits in large-scale production of hyperpolarized (129)Xe. Phys Rev A 2014; 90:023406.

48. Hersman FW, Ruset IC, Ketel S, et al. Large production system for hyperpolarized 129Xe for human lung imaging studies. Acad Radiol 2008; 15:683–692.

49. Roos JE, McAdams HP, Kaushik SS, et al. Hyperpolarized gas MR imaging: technique and applications. Magn Reson Imaging Clin North Am 2015; 23:217–229.

50. Altes TA, de Lange EE. Applications of hyperpolarized helium-3 gas magnetic resonance imaging in pediatric lung disease. TMRI 2003; 14:231–236.

51. Fain S, Schiebler ML, McCormack DG, et al. Imaging of lung function using hyperpolarized Helium-3 magnetic resonance imaging: review of current and emerging translational methods and applications. J Magn Reson Imaging 2010; 32:1398–1408.

52. Koumellis P, van Beek EJ, Woodhouse N, et al. Quantitative analysis of regional airways obstruction using dynamic hyperpolarized 3He MRI-preliminary results in children with cystic fibrosis. J Magn Reson Imaging 2005; 22:420–426.

53. Thomen RP, Walkup LL, Roach DJ, et al. Hyperpolarized 129Xe for investigation of mild cystic fibrosis lung disease in pediatric patients. J Cystic Fibrosis 2017; 16:275–282.

54. Kanhere N, Couch MJ, Kowalik K, et al. Correlation of lung clearance index with hyperpolarized 129Xe magnetic resonance imaging in pediatric subjects with cystic fibrosis. Am J Respir Crit Care Med 2017; 196:1073–1075.

55. Mets OM, Roothaan SM, Bronsveld I, et al. Emphysema is common in lungs of cystic fibrosis lung transplantation patients: a histopathological and computed tomography study. PloS ONE 2015; 10:e0128062.

56. Nguyen H, Cleveland ZI, Brody AS, et al. CT quantification of emphysema in children with cystic fibrosis with comparison to pulmonary function parameters. The International Pediatric Radiology 7th conjoint meeting and exhibition. Chicago, IL 2017.

57. Broström EB, Thunqvist P, Adenfelt G, et al. Obstructive lung disease in children with mild to severe BPD. Respir Med 2010; 104:362–370.

58. Spoel M, Marshall H, Ijsselstijn H, et al. Pulmonary ventilation and microstructural findings in congenital diaphragmatic hernia. Pediatr Pulmonol 2016; 51:517–524.

59. Cadman RV, Lemanske RF, Evans MD, et al. Pulmonary He-3 magnetic resonance imaging of childhood asthma. J Allergy Clin Immunol 2013; 131:369–376.

60. Fishman EF, Quirk JD, Sweet SC, et al. What makes a good pediatric transplant lung: insights from in vivo lung morphometry with hyperpolarized 3He magnetic resonance imaging. Pediatr Transplant 2017; 21: e12886- n/a.

61. Altes TA, Meyer CH, Mata JF, et al. Hyperpolarized helium-3 magnetic resonance lung imaging of non-sedated infants and young children: a proof-of-concept study. Clin Imaging 2017; 45:105–110.

62. Lord A, Shapiro AJ, Saint-Martin C, et al. Filamin A mutation may be associated with diffuse lung disease mimicking bronchopulmonary dysplasia in premature newborns. Respir Care 2014; 59:e171–e177.

63. Higano NS, Thomen R, Parks K, et al. Hyperpolarized 3He Gas MRI in Infant Lungs: Investigating Airspace Size. Annual meeting of the American Thoracic Society.; 2017. p. Washington, D.C.A2663.

64. Woods JC. The 129Xe MRI clinical trials consortium: a route for multi-site trials. The 2017 International Workshop on pulmonary imaging; 2017.